Acta Myologica • 2014; XXXIII: p. 22-33

2013 GAETANO CONTE PRIZE LECTURE

A gating model for wildtype and R1448H Nav1.4 channels in paramyotonia

Boris Holzherr, Frank Lehmann-Horn, Elza Kuzmenkina, Chunxiang Fan and Karin Jurkat-Rott

Division of Neurophysiology in the Center of Rare Diseases at Ulm University, Ulm, Germany

We studied the consequences of the Nav1.4 mutation R1448H that is situated in the fourth voltage sensor of the channel and causes paramyotonia, a cold-induced myotonia followed by weakness. Previous work showed that the mutation uncouples inactivation from activation. We measured whole-cell Na^+ currents at 10, 15, 20, and 25°C using HEK293 cells stably transfected with wildtype (WT) and R1448H Na^+ channels. A Markov model was developed the parameters of which reproduced the data measured on WT and R1448H channels in the whole voltage and temperature range. It required an additional transient inactivated state and an additional closed-state inactivation transition not previously described. The model was used to predict single-channel properties, free energy barriers and temperature dependence of rates. It allowed us to draw the following conclusions: i) open-state inactivation results from a two-step process; ii) the channel re-openings that cause paramyotonia originate from enhanced deactivation/reactivation and not from destabilized inactivation; iii) the closed-state inactivation of R1448H is strikingly enhanced. We assume that latter explains the episodic weakness following cold-induced myotonia.

Key words: Paramyotonia, markov model, sodium channel, closed-state inactivation, channelopathy, skeletal muscle

Introduction

Paramyotonia congenita (PC) is characterized by muscle stiffness provoked by exposure to cold and particularly by exercise in cold environment (1). During deep cooling the myotonia disappears and gives way to flaccid paralysis which may last several hours. Causative mutations are in the skeletal muscle sodium channel Nav1.4. Investigations of the biophysical alterations in channel gating due to PC mutations has revealed several gating defects consistent with membrane hyperexcitability. Mutant channels inactivate more slowly and with less voltage dependence than WT channels, deactivate more slowly, and exhibit a more rapid rate of recovery from fast inactivation (2). The very frequently occurring R1448H mutation which affects the outermost amino acid of the transmembrane segment S4 of domain DIV has been attributed to an uncoupling of fast inactivation from activation (3).

Voltage-gated Na^+ channels are essential for the generation of action potentials. They consist of four homologous domains (DI to DIV) which each contain six transmembrane segments (S1 to S6). At depolarization, the S4 segments, which contain several positive amino acid residues and therefore function as voltage sensors, can move outwardly and thereby alter channel confirmation and function. Different charge contents of the various S4 segments suggest that the charges have domain-specific functions. While S4 of DI and DII are thought to play a prominent role in Na^+ channel activation, S4 of DIII and DIV regulate fast inactivation (4). Finally, the pore with its selectivity filter is lined by the loops between S5 and S6 and the S5 and S6 segments itself.

Na^+ channel activation is a multi-step process which is usually implemented as a series of closed states leading to one or more open states. Generally, the distributions of single-channel open times follow a single exponential (5). Inactivation is coupled to activation (6). The voltage dependence of inactivation is supported by a significant gating current during fast inactivation (7) and can be used to describe voltage dependence of channel reopening and mean open times (8). The time course of fast inactivation is reported to be single-exponential as well as double-exponential which is either implemented as two open states (9) or by a two-step inactivation process (10). After reaching the fast inactivated state, Na^+ channels do not go immediately back to the closed states, repolarization of the membrane is necessary to initiate recovery.

Address for correspondence: Karin Jurkat-Rott, Division of Neurophysiology, Ulm University, Albert-Einstein-Allee 11, 89081 Ulm, Germany. E-mail: karin.jurkat-rott@uni-ulm.de

To account for recovery from fast inactivation, which is not occurring by re-entering the open state (11), models were expanded with transitions between inactivated and closed states (12). As inactivation occurs from open as well as from closed states, and recovery from fast inactivation develops with a delay (13), multiple inactivation states are assumed.

Since low temperature is the trigger for paramyotonia, temperature effects have been studied and shown to affect both the kinetic and steady-state parameters of Nav1.4 WT and R1448H channels. This is not surprising, given that each of the voltage-dependent gating steps is likely to involve different conformational changes in the channel and so require the breaking and/or forming of chemical bonds with different energies. However, data obtained at room temperature cannot be extrapolated to physiological temperatures using a single temperature scaling factor. Therefore measurements in a wide temperature range and a suitable gating model which is valid in a large potential and temperature range are required to study R1448H. In the present study, we characterized the gating of Nav1.4 WT and R1448H mutant channels with the whole-cell configuration of the patch-clamp technique between 5 and 30 °C. Also, we determined parameters of a Markov model which was able to fit the measurements at all potentials and temperatures. The model was then used to predict gating currents and single-channel properties.

Materials and methods

Na^+ channel expression

WT and mutant (R1448H) α-subunit constructs of human skeletal muscle Na^+ channels were assembled in the mammalian expression vector pRC/C MV and transfected into human embryonic kidney cells (HEK 293) by the calcium phosphate precipitation method. Since transient expression was low (< 10%) stable cell lines were obtained by antibiotic selection as previously described (14).

Recording techniques

Whole-cell currents were recorded using an Axopatch 200A patch-clamp amplifier (Molecular Devices, USA). Signal acquisition and processing was done using the DigiData card (1200) and pCLAMP (V6) software (Molecular Devices, USA). Whole-cell currents were filtered at 10 kHz, and digitized at 10 or 20 μs. Patch pipettes were pulled on a Zeitz Puller (Zeitz Instruments, Martinsried, Germany). Pipette resistance ranged from 0.8 to 1.2 MΩ. The extracellular recording solution was (in mM): 150 NaCl, 2 KCl, 1.5 $CaCl_2$, 1 $MgCl_2$ and 10 HEPES, titrated to pH 7.4 with NaOH. The pipette solution was (in mM): 105 CsF, 35 NaCl, 10 EGTA and 10 HEPES, titrated to pH 7.4 with CsOH. After achieving the whole-cell configuration, cells were held for 10 min at -120 mV to ensure proper diffusion of the pipette solution into the cell and to stabilize of the Na^+ current amplitude. Recording temperature was maintained between 5 and 30°C by a Peltier device and a HC-100A temperature controller (Dagan, USA). To avoid evaporation at high temperatures and dilution by condensation at low temperatures, the bath solution was continuously exchanged by a gravity driven perfusion system.

Electrophysiological protocols and data analysis

Voltage dependence of activation was obtained by a series of 50 ms depolarizing pulses from a holding potential of -140 mV ranging from -85 to 55 mV and steady-state fast inactivation was obtained by 200 ms conditioning pulses from -150 to -45 mV from a holding potential of -140 mV followed by a test pulse to -15 mV. Activation and steady-state fast inactivation curves were fit with standard Boltzmann function as previously described (15). Time constants of fast inactivation were obtained by fitting double-exponential functions to the decaying part of the current traces obtained with the activation protocol. Because the fast component accounted for > 90% of the current amplitude, macroscopic inactivation of the Na^+ current was quantified by the fast component only. Time course of entry into fast inactivation (closed-inactivation) was obtained by a double pulse protocol. From a holding potential of -140 mV a conditioning pulse V_{cond} (-100, -90, -80, -70 mV) for increasing durations (from 0.1 to 300 ms) was applied in order to inactivate Na^+ channels without opening. The conditioning pulse was followed by a test pulse to -15 mV to determine the fraction of non-inactivated channels. Time course of entry into fast inactivation was obtained by fitting a single exponential function to the normalized curve. Recovery from fast inactivation was determined by a double pulse protocol. A 150 ms pulse to -15 mV was used to inactivate all Na^+ channels. A test pulse to -15 mV followed after an increasing interval (from 0.025 to 250 ms) at the recovery potential (-140, -120 and -100 mV). Time course of recovery from fast inactivation was obtained by fitting single/double exponential function to the normalized curve.

Curve fits and data analysis were performed with pCLAMP 8.0 (Molecular Devices), Excel (Microsoft, Inc. Redmond, WA), and Origin (MICROCAL Software, Inc., Northhampton, MA). Differences from WT and mutant were considered as significant at $p < 0.05$ (Student's t-test). Grouped data are presented as mean ± SEM. SEM is represented in graphs as bars when in exceeds the size of the symbol.

Sodium channel gating model

Recordings from activation, steady-state fast inactivation, entry into closed-state inactivation and recovery from fast inactivation were simultaneously fit to a gating model using an advanced version of IonFit software (16). Model parameters were optimized using the least squares method. Ionic currents were simulated by solving master equations of a continuous-time Markov process,

$$\frac{d}{dt}P_i(t) = \sum_j r_{ji}(V)P_j(t) - r_{ij}(V)P_i(t) \quad (1),$$

whereby $P_i(t)$ denotes the population of state i at a given time t, and $r_{ij}(V)$ denotes the rate constant for the transition from state i to j. The voltage dependent forward $r_{ij}(V)$ and backward $r_{ji}(V)$ transition rates between state i and j were assumed to be single-exponential functions of voltage (17),

$$r_{ij}(V) = r'_{ij} \cdot exp\left(\frac{zxr_{ij} \cdot FV}{RT}\right) \quad (2),$$

$$r_{ji}(V) = r'_{ji} \cdot \exp\left(\frac{-zxr_{ji} \cdot FV}{RT}\right) \quad (3)$$

whereby zxr_{ij} and zxr_{ji} represent the effective charge moving from an original state to the barrier peak, as a product of the total charge moved and the fraction of the electric field where the barrier peak was located. r'_{ij} and r'_{ji} represent the rate constants at 0 mV, including enthalpic and entropic factors. F represents the Faraday constant, R the ideal gas constant, V the membrane potential and T the absolute temperature. The initial state populations were determined as a steady-state solution of Eq. 1 at a holding potential V_{hold} with $dP_i(t)/dt=0$. For steady-state fast inactivation curve, recovery from fast inactivation and entry into fast inaction, currents were simulated according to the pulse protocols and the respective current peak amplitudes were determined. Data sets used to determine model parameters consisted of six current traces for test pulses of -40 to 10 mV, the steady state inactivation curve between -160 and -45 mV, time course of entry into fast inactivation at four different prepulse potentials (-100 to -70 mV) and time course of recovery from fast inactivation at three different recovery potentials (-140 to -100 mV).

To describe the energy profile, the rate constants in Eq. 2 and Eq. 3 were written with explicit entropic ΔS and enthalpic ΔH terms. The voltage independent parts are equal to the pre-factors r'_{ij} and r'_{ji},

$$r'_{ij}(T) = \frac{k_B T}{h} \cdot exp\left(\frac{-\Delta H_{r_{ij}} + T\Delta S_{r_{ij}}}{RT}\right) \quad (4)$$

$$r'_{ji}(T) = \frac{k_B T}{h} \cdot exp\left(\frac{-\Delta H_{r_{ji}} + T\Delta S_{r_{ji}}}{RT}\right) \quad (5)$$

and can be used to determine ΔH and ΔS.

Rate constants were used to calculate single channel properties. If a channel opens, the number of openings before inactivation follows a geometric distribution (18), the mean of which may be calculated from the model's rate constants

$$N = \frac{1}{1 - \left(\frac{\alpha_2}{\alpha_3 + \alpha_2 + \beta_1}\right) \cdot \left(\frac{\beta_2}{\alpha_6 + \beta_2}\right)} \quad (6)$$

The mean open time τ_O of single channels of the model was estimated by the reciprocal sum of the rates leaving the open state

$$\tau_O = \frac{1}{\alpha_6 + \beta_2} \quad (7)$$

To test the hypothesis of an increased probability of $O \rightarrow C_4 \rightarrow I_2$ transitions, the steady-state probability was calculated by

$$P(O \rightarrow C_4 \rightarrow I_2) = \frac{\beta_2}{\beta_2 + \alpha_6} \cdot \frac{\alpha_3}{\alpha_3 + \alpha_2 + \beta_1} \quad (8)$$

It is very likely that there are variations in basic properties of channel population from cell to cell, and this variation may mimic the real variation seen in native preparations. For this reason all fits and simulations were done by using data of individual cells and results were pooled afterwards.

Results

Whole-cell currents

At all temperatures activation kinetics and sodium currents decay were slower for R1448H than for WT (Fig. 1A). Cooling from 30°C to 10°C slowed kinetics ~10-fold and reduced peak current amplitudes to a quarter for both WT and mutant channels (Fig. 1B). In contrast, cooling increased the total sodium influx into the cell by different amounts: at 10°C in relation to 30°C, the area under the curve was multiplied by a factor of two for WT and by a factor of four for R1448H (Fig. 1C).

Steady-state activation curves were almost identical for WT and R1448H regardless of temperature (Fig. 2A, Table 1). Cooling decreased activation slope factor from ~-7mV to ~-10mV and potentials at half maximal activation were shifted by ~+8 mV to the right for WT

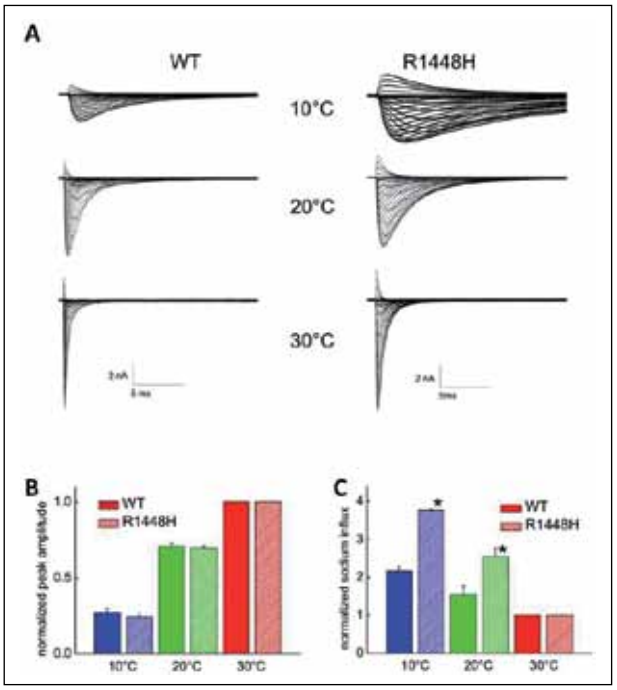

Figure 1. A Raw data. Representative whole-cell current traces recorded at different temperatures from HEK293 cells stably expressing either WT (left) or R1448H (right) mutant channels: 10°C (top), 20°C (middle) and 30°C (bottom). Note the slowed inactivation of the mutant. B Temperature effect on amplitude. Temperature dependency of currents through WT or R1448H Nav1.4 channels normalized to values at 30°C. C Temperature effect on flux. Temperature dependency of Na^+ influx through WT or R1448H Nav1.4 channels. For B and C, values are mean ± SEM (n = 6). SEM is shown as bars and * indicates a significant difference between WT and R1448H (p < 0:05). Note that while the amplitude shows similar temperature dependence, the flux of the mutant is increased due to the slowed inactivation.

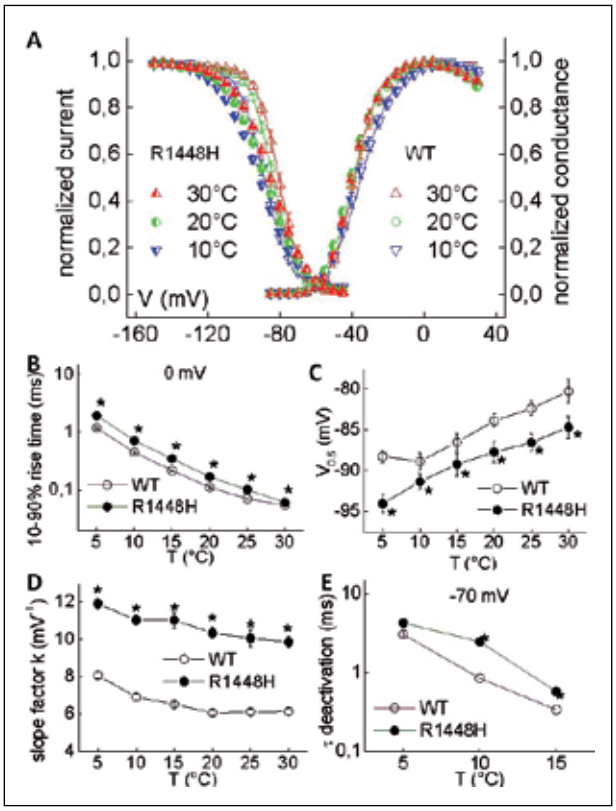

Figure 2. A Activation and steady-state fast inactivation. Activation and steady-state fast inactivation curves for WT and R1448H. Voltage dependence of activation was determined by 50 ms depolarizing pulses to the indicated potentials from a holding potential of -140 mV. Steady-state inactivation curve was determined with a 200 ms prepulse to the indicated potentials prior to a 10 ms test pulse to -15 mV (-140 mV holding potential). Solid lines represent fits to standard Boltzmann functions. Note that activation is similar but inactivation is changed for the mutant. B Rise time. 10-90% rise time as a measure for activation WT and R1448H. Note the slower kinetics of the mutant. C and D parameters of inactivation. Temperature dependence of Boltzmann parameters of WT and R1448H for steady-state fast inactivation. Note the left-shift (more negative $V_{0.5}$) and decreased steepness (larger k value) of the mutant. E Deactivation time constant. Comparison of deactivation time constants at -70 mV, the only potential with a significant difference. Note the accelerated kinetics of the mutant. For A to E, all values are mean ± SEM (n = 8-30). SEM is shown as bars when it exceeds the size of the symbol and * indicates a significant difference between WT and R1448H (p < 0:05).

and R1448H alike. Rise time of activation at 0 mV and higher was significantly increased in R1448H compared to WT ($p \leq 0.05$, Fig. 2B). Steady-state inactivation differed significantly ($p = 0.05$) for the mutant as well: R1448H curves were significantly shifted to the left by ~6 mV and revealed an increase of slope factor by ~4 mV (Fig. 2A, C, D, Table 1). Since deactivation cannot be measured at room temperature, we cooled to 15°C, 10°C and 5°C to resolve sufficient data points for a fit. Deactivation time course was almost indistinguishable for mutant and WT except for the near-threshold voltage of -70 mV (Fig. 2E).

For threshold-near potentials, the time constants of fast inactivation T_h form the open state were smaller for R1448H than WT while at more depolarized potentials, they were larger than for WT (Fig. 3: OSI). The difference in time constants was especially prominent in the voltage range of -60 to -30 mV and markedly increased with cooling. Cooling slowed fast inactivation of WT and R1448H at all voltages tested and shifted the point of intersection of WT and R1448H curves to more negative potentials.

Table 1. Boltzmann parameters of G(V) and SSFI curves.

°C		5	10	15	20	25	30
WT *G*(V)	$V_{0.5}$(mV) k(mV) n	-31.7 ± 1.6 -9.7 ± 0.2 8	-35.7 ± 1.4† -8.3 ± 0.2† 13	-36.8 ± 1.0 -7.8 ± 0.1 20	-38.8 ± 0.7 -7.2 ± 0.1 30	-40.4 ± 1.0 -6.8 ± 0.2 19	-37.6 ± 1.2 -6.6 ± 0.3† 14
R1448H *G*(V)	$V_{0.5}$(mV) k(mV) n	-31.3 ± 1.3 -9.6 ± 0.2 13	-37.0 ± 1.0† -8.3 ± 0.2† 18	-38.3 ± 0.7 -8.0 ± 0.1 12	-40.3 ± 0.7 -7.3 ± 0.1 19	-41.5 ± 1.1 -6.9 ± 0.3 10	-39.4 ± 0.5 -7.0 ± 0.1 14
WT SSFI	$V_{0.5}$(mV) k(mV) n	-88.2 ± 0.7 8.06 ± 0.2 8	-87.3 ± 0.7† 6.8 ± 0.2† 13	-84.8 ± 0.4 6.4 ± 0.1 19	-83.0 ± 0.5 6.1 ± 0.1 30	-82.4 ± 0.9 6.1 ± 0.1 19	-79.9 ± 1.0† 6.2 ± 0.1 14
R1448H SSFI	$V_{0.5}$(mV) k(mV) n	-93.7 ± 1.1* 12.0 ± 0.3* 13	-91.0 ± 0.8*† 10.7 ± 0.2*† 18	-88.7 ± 1.2* 10.8 ± 0.3* 12	-87.0 ± 1.1* 10.1 ± 0.2* 18	-86.7 ± 1.1* 9.9 ± 0.4* 10	-85.0 ± 1.3* 9.5 ± 0.3* 14

* indicates a significant difference between WT and R1448H at the same temperature, † indicates a significant difference between 10, 20 and 30°C, ($p < 0:05$).

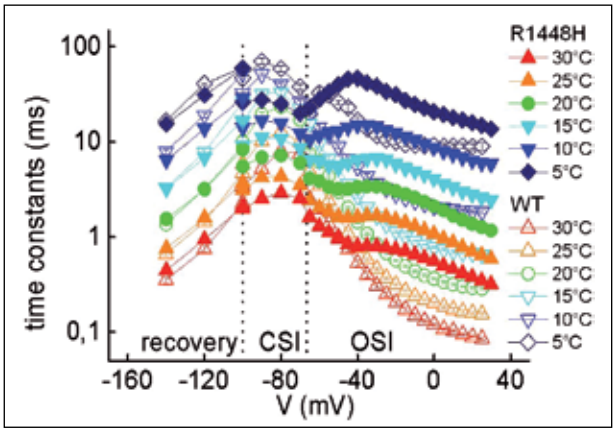

Figure 3. Time constants. Time constants from and into the fast inactivated-state were plotted against the corresponding membrane potentials. Recovery, entry (Closed-state inactivation, CSI) and inactivation from the open-state (OSI) were determined for WT and R1448H between 5 and 30°C. Values are mean ± SEM (n = 5-30). SEM is shown as bars when it exceeds the size of the symbol and * indicates a significant difference between WT and R1448H ($p < 0:05$). Note the accelerated CSI and slowed OSI of the mutant at all temperatures, while the recovery is indistinguishable.

Additionally, R1448H reduced voltage dependence of T_h for all temperatures tested.

R1448H accelerated entry into closed-state inactivation (CSI) by about two-fold on average (Fig. 3: CSI, Table 2). The left-shift of the steady-state inactivation curve may explain this enhanced closed-state inactivation. The mutation reduced its voltage dependence, possibly by the removed S4 charge, and slowed the open-state inactivation. Finally, R1448H showed a tendency to recover more rapidly without reaching significant levels (Fig. 3: recovery, Table 3). However, neither the delay in onset to recovery nor its voltage and temperature dependence were altered by R1448H.

Gating model

The gating model used in the present study consisted of a series of four closed states C_1-C_4, one open state O and four inactivated states I_1-I_3 and I_T (Fig. 4). By convention, all transitions towards O have positive valences because they are favored by depolarization, while those away from O have negative valences because they are favored by repolarization. Rate constants between the closed states and rate constants between C_3-C_4-O and I_1-I_2-I_3 were assumed to be equal to reduce the number of free parameters. The model is based on previous models of Vandenberg and Bezanilla (19). However, to properly describe gating of WT and R1448H and their temperature dependence, two modifications were made. First, we introduced a transient inactivated state I_T as previously suggested by Kahlig et al. (10) to account for the biphasic inactivation especially at low temperatures. Second, we introduced a transition between C_4 and I_2. This transition was essential to reproduce inactivation from closed states especially in the voltage range around threshold of Na^+ channels.

The model was able to reproduce all measurements including the strong voltage dependence of channel activation, open and closed state inactivation, recovery and temperature dependence (Fig. 5). The model resulted in rate constants of WT and R1448H which were similar for most transitions (Tables 4 and 5). However the rate constants alpha3, beta3 and alpha6 markedly differed

Table 2. Time constants of entry into fast inactivation.

°C		5	10	15	20	25	30
WT	$\tau_{entry-100}$(ms)	47.0 ± 7.4	32.5 ± 3.8†	16.1 ± 1.6	10.1 ± 1.3	5.9 ± 0.8	3.4 ± 0.7†
	n	8	15	18	22	15	8
	$\tau_{entry-90}$(ms)	70.8 ± 4.8	51.3 ± 2.7†	31.9 ± 1.9	19.7 ± 0.9	10.3 ± 0.5	5.2 ± 0.7†
	n	7	15	20	24	15	9
	$\tau_{entry-80}$(ms)	58.7 ± 4.0	40.4 ± 2.4†	32.9 ± 2.1	23.5 ± 0.9	12.9 ± 0.7	8.0 ± 0.5†
	n	7	15	20	24	15	9
	$\tau_{entry-70}$(ms)	38.1 ± 2.6	26.2 ± 1.8†	22.1 ± 1.4	17.1 ± 1.0	10.0 ± 0.8	7.6 ± 0.8†
	n	7	13	20	22	14	9
R1448H	$\tau_{entry-100}$(ms)	26.4 ± 1.2*	14.1 ± 0.7*†	9.2 ± 0.5*	5.5 ± 0.3*	3.2 ± 0.2*	2.0 ± 0.2†
	n	10	18	12	17	10	9
	$\tau_{entry-90}$(ms)	27.8 ± 0.9*	17.0 ± 0.7*†	11.2 ± 0.5*	6.9 ± 0.3*	4.3 ± 0.2*	2.6 ± 0.1*†
	n	10	18	12	16	9	9
	$\tau_{entry-80}$(ms)	25.3 ± 0.7*	15.8 ± 0.6*†	10.9 ± 0.5*	7.2 ± 0.2*	4.4 ± 0.1*	2.9 ± 0.2*†
	n	10	18	12	17	9	9
	$\tau_{entry-70}$(ms)	20.1 ± 0.7*	12.3 ± 0.5*†	8.7 ± 0.4*	6.0 ± 0.2*	3.5 ± 0.1*	2.6 ± 0.2*†
	n	10	18	12	17	8	9

* indicates a significant difference between WT and R1448H at the same temperature, † indicates a significant difference between 10, 20 and 30°C, (p < 0:05).

Table 3. Time constants of recovery from fast inactivation.

°C		5	10	15	20	25	30
WT(-140 mV)	τ_{rec_1}(ms)	16.61 ± 0.49	7.94 ± 0.42†	3.28 ± 0.11	1.37 ± 0.04	0.66 ± 0.03	0.35 ± 0.03†
	τ_{rec_2}(ms)	-	-	34.6 ± 3.8	24.5 ± 2.2	19.1 ± 1.4	16.6 ± 0.8
	delay (ms)	1.54 ± 0.03	0.81 ± 0.04†	0.57 ± 0.01	0.31 ± 0.01	0.18 ± 0.01	0.1 ± 0.003†
	n	6	14	17	19	10	9
R1448H(-140 mV)	τ_{rec_1}(ms)	15.50 ± 1.79	6.45 ± 0.28†	3.23 ± 0.14	1.55 ± 0.08	0.76 ± 0.04	0.45 ± 0.04†
	τ_{rec_2}(ms)	-	-	39.3 ± 4.1	32.8 ± 3.6	21.1 ± 1.3	21.5 ± 1.9
	delay (ms)	1.79 ± 0.25	0.84 ± 0.03†	0.58 ± 0.02	0.3 ± 0.01	0.19 ± 0.02	0.099 ± 0.003†
	n	9	17	12	18	7	7
WT(-120 mV)	τ_{rec_1}(ms)	40.92 ± 1.09	19.14 ± 1.16†	7.81 ± 0.36	3.21 ± 0.11	1.45 ± 0.09	0.75 ± 0.06†
	τ_{rec_2}(ms)	-	-	63.1 ± 6.7	50.2 ± 5.6	38.2 ± 3.2	36.0 ± 3.0
	delay (ms)	3.26 ± 0.07	1.51 ± 0.10†	1.03 ± 0.02	0.55 ± 0.02	0.29 ± 0.01	0.15 ± 0.01†
	n	6	14	18	19	10	9
R1448H(-120 mV)	τ_{rec_1}(ms)	31.44 ± 3.26*	13.86 ± 0.66*†	6.88 ± 0.28	3.18 ± 0.18	1.60 ± 0.16	0.95 ± 0.07*†
	τ_{rec_2}(ms)	-	-	79.5 ± 15.9	51.8 ± 6.8	39.4 ± 3.4	47.8 ± 3.5
	delay (ms)	3.34 ± 0.48	1.45 ± 0.05†	0.97 ± 0.04	0.57 ± 0.02	0.30 ± 0.01	0.14 ± 0.01†
	n	9	17	10	18	6	7
WT(-100 mV)	$\tau_{rec\_}$ (ms)	59.97 ± 2.89	52.82 ± 2.90†	26.21 ± 1.40	9.08 ± 0.35	4.72 ± 0.34	2.27 ± 0.24†
	τ_{rec_2}(ms)	-	-	-	58.2 ± 5.8	98.6 ± 26.2	96.0 ± 18.5
	delay (ms)	4.20 ± 0.15	3.31 ± 0.23†	1.93 ± 0.07	1.10 ± 0.04	0.56 ± 0.03	0.33 ± 0.04†
	n	5	13	19	16	8	10
R1448H(-100 mV)	τ_{rec_1}(ms)	59.30 ± 3.32	29.17 ± 1.43*†	16.85 ± 0.86*	8.36 ± 0.43	3.75 ± 0.30	2.10 ± 0.11†
	τ_{rec_2}(ms)	-	-	-	-	53.2 ± 4.4	110.8 ± 19.5
	delay (ms)	6.01 ± 0.78	3.14 ± 0.19†	1.79 ± 0.14	0.96 ± 0.06	0.58 ± 0.05	0.27 ± 0.03†
	n	8	17	12	17	6	8

* indicates a significant difference between WT and R1448H at the same temperature, † indicates a significant difference between 10, 20 and 30°C, (p < 0:05).

between WT and R1448H. The smaller alpha6 explains the impaired fast inactivation of R1448H. The most striking difference between WT and mutant related to alpha3 and beta3, the transition between C4 and I2. In contrast to the WT for which the calculated rate constants suggest that this transition does not occur, the mu-

tant performed this closed-state inactivation transition with a high likelihood.

Effective charge movement increased with temperature for all transitions in both WT and R1448H by about 30%. For example the equivalent gating charge for opening the channels from rest was 5.31 to 6.78 e0 for WT and 4.39 to 5.56 e0 for mutant, obtained by summing the charges for each of the four transitions from C1 to O (values dependent on voltage, Table S6). Most of the charge movement in the activation pathway was concentrated in the last transition (C4-O) 2.58 ± 0.06 to 3.06 ± 0.04 e0 for WT and 2.53 ± 0.05 to 2.98 ± 0.09 e0 for mutant. We interpret this finding so that this transition may represent several steps in one the final of which may really be voltage-independent. In general, effective charge movement for transitions from inactivated to closed states during recovery were notably larger compared to their respective forward rates during closed-state inactivation accounting for the strong voltage dependence of recovery from inactivation. For the mutant the equivalent gating charge movement during recovery was smaller than for WT leading to reduced voltage dependence. About 50% of total gating charge of WT and 40% of charge for the mutant was immobilized by fast inactivation.

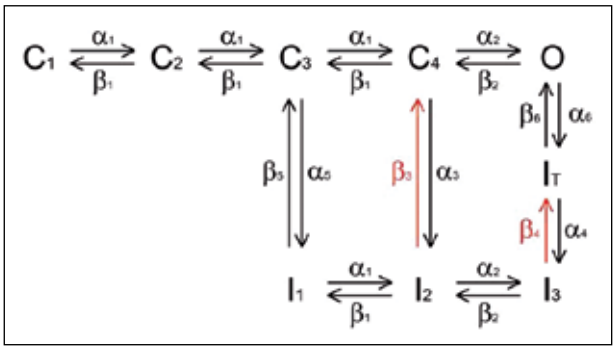

Figure 4. Gating model. Gating model used for kinetic simulations, consists of 4 closed-states C1–C4, one open- state O, four inactivated-states I1–I3 and IT. Arrows between states indicate possible transitions and _i and _i (i=1..6) represent the voltage-dependent rate constants. Rate constants _3 and _4 were calculated based on microscopic reversibility. Note the additional transient inactivated state IT and the transition C4-I2 both of which have not been previously used.

Free energy barriers

The energy changes involved in the transitions between the closed-states (C1–C2–C3–C4) and the paral-

Table 4. Model parameters for WT.

Transition	Parameter	10°C	15°C	20°C	25°C
C – C and I_1 – I_2	zxα1	0.1957 ± 0.0020	0.1882 ± 0.0132	0.1716 ± 0.0153	0.1678 ± 0.0125
	α1	7.75e03 ± 3.10e02	1.25e04 ± 1.96e02	2.27e04 ± 3.30e02	3.36e04 ± 1.18e03
	zxβ1	-0.7134 ± 0.0144	-0.8312 ± 0.0205	-0.9831 ± 0.0166	-1.0712 ± 0.0167
	β	1.61e03 ± 6.90e01	1.88e03 ± 1.09e02	1.87e03 ± 1.09e02	2.19e03 ± 6.99e01
C_4 – O and I_2 – I_3	zx α2	1.9079 ± 0.0422	1.9649 ± 0.0323	1.9775 ± 0.0164	1.8978 ± 0.0341
	α2	2.80e04 ± 1.46e03	6.37e04 ± 3.65e03	1.43e05 ± 8.41e03	3.50e05 ± 1.30e04
	zxβ2	-0.6711 ± 0.0374	-0.8309 ± 0.0596	-0.9167 ± 0.0307	-1.1666 ± 0.0289
	β2	5.93e01 ± 5.17e00	1.88e02 ± 4.02e01	5.70e02 ± 2.44e01	2.03e03 ± 3.29e01
C_4 – I_2	zxα3	0.0001 ± 0.0001	0.0153 ± 0.0122	0.0552 ± 0.0475	0.0310 ± 0.0201
	α3	5.40e-07 ± 1.61e-07	5.56e-06 ± 1.53e-06	3.14e-05 ± 1.57e-05	5.14e-04 ± 1.39e-04
	zxβ3	-1.0982 ± 0.0034	-1.2190 ± 0.0254	-1.3437 ± 0.0406	-1.5462 ± 0.0251
	β3	3.47e-10 ± 1.09e-10	3.81e-09 ± 1.16e-09	2.22e-08 ± 1.35e-08	2.74e-07 ± 6.99e-08
I_T – I_3	zxα4	0.0004 ± 0.0002	0.0140 ± 0.0123	0.0207 ± 0.0160	0.0004 ± 0.0002
	α4	5.36e01 ± 5.63e00	1.19e02 ± 8.12e00	2.48e02 ± 1.06e01	5.46e02 ± 1.71e01
	zxβ4	-0.8464 ± 0.0113	-0.8826 ± 0.0349	-0.9534 ± 0.0291	-1.0731 ± 0.0304
	β4	8.56e-01 ± 1.76e-01	3.30e00 ± 4.11e-01	1.45e01 ± 2.02e00	4.79e01 ± 4.51e00
C_3 – I_1	zxα5	0.0016 ± 0.0006	0.0040 ± 0.0026	0.0113 ± 0.0076	0.0123 ± 0.0107
	α5	3.78e02 ± 1.76e01	4.74e02 ± 2.30e01	4.92e02 ± 2.26e01	6.89e02 ± 2.06e01
	zxβ5	-1.0967 ± 0.0032	-1.2302 ± 0.0258	-1.3877 ± 0.0310	-1.5650 ± 0.0088
	β5	2.40e-01 ± 1.70e-02	3.06e-01 ± 3.96e-02	3.19e-01 ± 4.81e-02	3.73e-01 ± 1.60e-02
O – I_T	zxα6	0.2514 ± 0.0098	0.3349 ± 0.0148	0.4063 ± 0.0258	0.4692 ± 0.0131
	α6	5.29e02 ± 2.24e01	1.42e03 ± 5.73e01	3.08e03 ± 1.06e02	6.05e03 ± 3.12e01
	zxβ6	-0.0002 ± 0.0001	-0.0027 ± 0.0016	-0.0185 ± 0.0164	-0.0345 ± 0.0164
	β6	2.40e01 ± 2.24e00	3.27e01 ± 1.47e00	3.37e01 ± 1.40e00	3.90e01 ± 2.65e00
	n	7	8	6	9

Model parameters αi and β i (i = 1..6) are the corresponding forward and backward transition rate constants at 0 mV. Parameters zxαi and zxβi are the valences of the corresponding transitions and reflect the voltage dependence of transition rates.* indicates a significant difference between WT and mutant (p < 0:05).

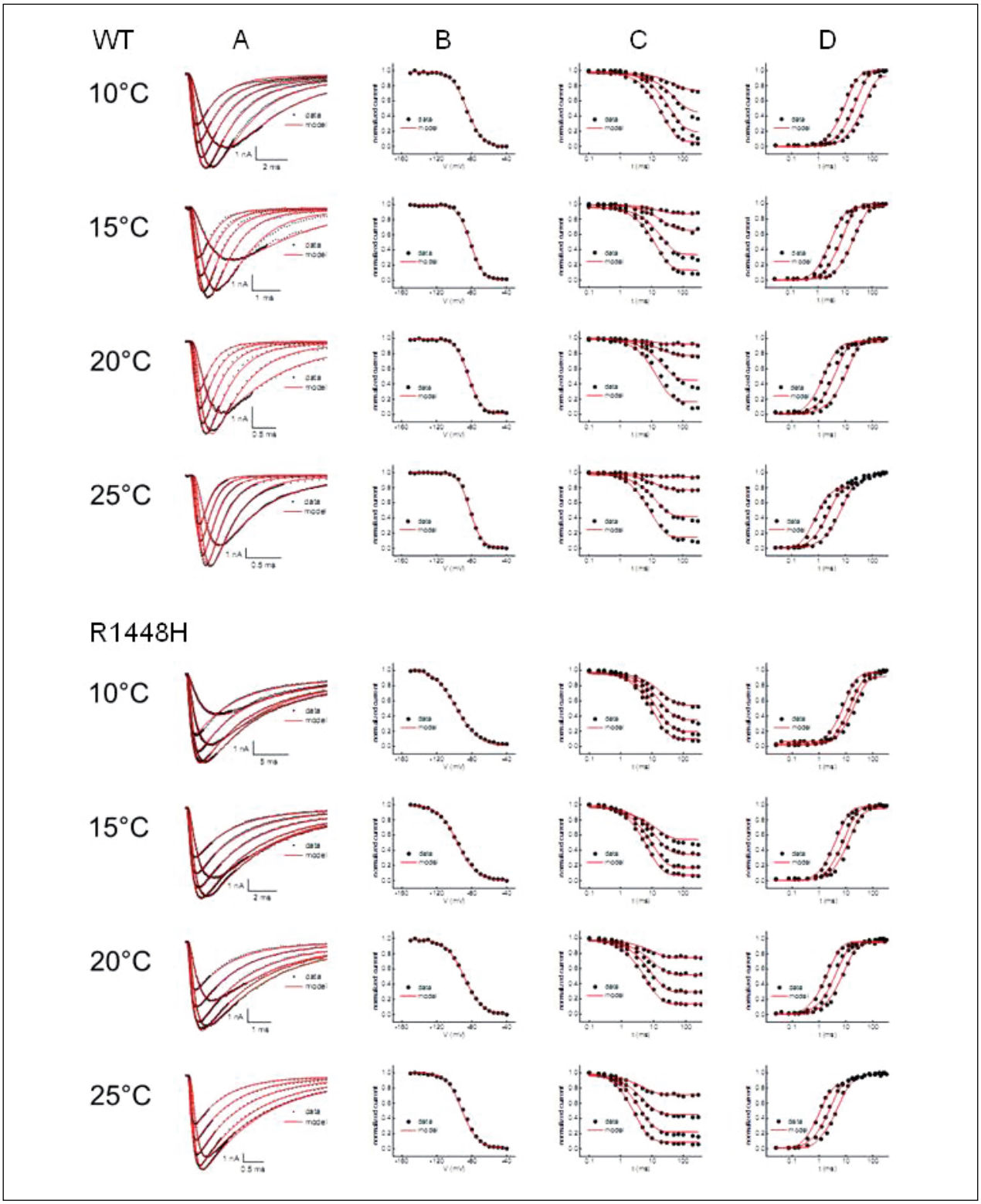

Figure 5. Representative current traces and fits. Original data at 10 to 25°C (black dots) are superimposed with fits of the model (red lines) obtained by simultaneous fitting of A) a series of 6 current traces elicited by pulses from -40 to 10 mV, (B) the steady-state fast inactivation curve determined in the range between -150 and -40 mV, (C) the time course of entry into fast inactivation at prepulse potentials of -100, -90, -80 -70 mV and (D) the time course of recovery from fast inactivation at recovery potentials of -140, -120, -100 mV for WT (top) and R1448H (bottom). Note the quality of the fits.

Table 5. Model parameters for R1448H.

Transition	Parameter	10°C	15°C	20°C	25°C
C – C and $I_1 – I_2$	zxα1	0.1339 ± 0.0145*	0.1122 ± 0.0083*	0.1264 ± 0.0129*	0.1166 ± 0.0165*
	α1	7.18e03 ± 1.61e02	1.27e04 ± 4.12e02	2.26e04 ± 7.90e02	3.62e04 ± 1.60e03
	zxβ1	-0.4894 ± 0.0168*	-0.6171 ± 0.0192*	-0.6763 ± 0.0177*	-0.7396 ± 0.0245*
	β	3.06e03 ± 1.14e02*	4.06e03 ± 1.77e02*	4.97e03 ± 9.29e01*	6.09e03 ± 5.45e02*
C_4 – O and $I_2 – I_3$	zx α2	1.8584 ± 0.0441	1.8970 ± 0.0513	1.9001 ± 0.0469	1.8041 ± 0.0828
	α2	2.93e04 ± 1.60e03	7.08e04 ± 6.47e03	1.52e05 ± 7.35e03	4.27e05 ± 3.24e04*
	zxβ2	-0.6685 ± 0.0310	-0.7235 ± 0.0472	-0.8106 ± 0.0200*	-1.1766 ± 0.0449
	β2	2.46e01 ± 2.65e00*	1.09e02 ± 5.04e00*	3.73e02 ± 2.25e01*	1.06e03 ± 1.70e02*
$C_4 – I_2$	zxα3	0.0027 ± 0.0010	0.0291 ± 0.0278	0.0009 ± 0.0003	0.0036 ± 0.0020
	α3	7.50e02 ± 3.55e01*	8.37e02 ± 5.29e01*	8.07e02 ± 4.37e01*	1.07e03 ± 4.22e01*
	zxβ3	-0.9188 ± 0.0187*	-0.9477 ± 0.0324*	-1.0421 ± 0.0270*	-1.2099 ± 0.0254*
	β3	1.19e00 ± 1.17e-01*	1.28e00 ± 1.65e-01*	1.39e00 ± 1.69e-01*	1.92e00 ± 2.54e-01*
$I_T – I_3$	zxα4	0.0051 ± 0.0024	0.0022 ± 0.0012	0.0135 ± 0.0124	0.0009 ± 0.0003
	α4	3.53e01 ± 3.88e00*	5.53e01 ± 2.73e00*	1.39e02 ± 1.91e01*	1.87e02 ± 8.12e00*
	zxβ4	-0.6289 ± 0.0176*	-0.6326 ± 0.0283*	-0.6043 ± 0.0322*	-0.7623 ± 0.0335*
	β4	4.28e-01 ± 5.99e-02*	1.12e00 ± 1.35e-01*	5.91e00 ± 1.21e00*	1.38e01 ± 2.93e00*
$C_3 – I_1$	zxα5	0.0036 ± 0.0024	0.0020 ± 0.0011	0.0001 ± 0.0001	0.0013 ± 0.0008
	α5	5.34e02 ± 7.97e01	7.25e02 ± 6.43e01*	8.75e02 ± 3.03e01*	1.08e03 ± 5.57e01*
	zxβ5	-0.9179 ± 0.0183*	-0.9749 ± 0.0147*	-1.0429 ± 0.0270*	-1.2121 ± 0.0247*
	β5	8.03e-01 ± 8.72e-02*	1.06e00 ± 8.29e-02*	1.52e00 ± 1.94e-01*	1.89e00 ± 1.89e-01*
O – I_T	zxα6	0.2861 ± 0.0071*	0.3328 ± 0.0086	0.4250 ± 0.0110	0.4500 ± 0.0129
	α 6	1.16e02 ± 7.78e00*	2.61e02 ± 1.04e01*	5.56e02 ± 1.47e01*	1.03e03 ± 3.54e01*
	zxβ6	-0.0015 ± 0.0012	0.0093 ± 0.0092	-0.0002 ± 0.0001	-0.0001 ± 0.0001
	β6	1.61e01 ± 2.11e00*	2.01e01 ± 1.54e00*	2.39e01 ± 2.96e00*	2.75e01 ± 3.06e00*
	n	8	8	8	6

Model parameters αi and β i (i = 1..6) are the corresponding forward and backward transition rate constants at 0 mV. Parameters zxαi and zxβi are the valences of the corresponding transitions and reflect the voltage dependence of transition rates.* indicates a significant difference between WT and mutant (p < 0:05).

Table 6. Equivalent gating charges.

WT	Transitions	No	10 °C	15 °C	20 °C	25°C
	C – C and $I_1 – I_2$	1	0.91 ± 0.01	1.02 ± 0.02	1.15 ± 0.02	1.24 ± 0.02
	C_4 – O and $I_2 – I_3$	2	2.58 ± 0.06	2.80 ± 0.07	2.89 ± 0.03	3.06 ± 0.04
	$C_4 – I_2$	3	1.10 ± 0.01	1.23 ± 0.03	1.40 ± 0.06	1.58 ± 0.03
	$I_T – I_3$	4	0.85 ± 0.01	0.90 ± 0.04	0.97 ± 0.03	1.07 ± 0.03
	$C_3 – I_1$	5	1.10 ± 0.01	1.23 ± 0.03	1.40 ± 0.03	1.58 ± 0.01
	O – I_T	6	0.25 ± 0.01	0.34 ± 0.01	0.42 ± 0.03	0.50 ± 0.02
R1448H	Transitions	No	10 °C	15 °C	20 °C	25°C
	C – C and $I_1 – I_2$	1	0.62 ± 0.02	0.73 ± 0.02	0.80 ± 0.02	0.86 ± 0.03
	C_4 – O and $I_2 – I_3$	2	2.53 ± 0.05	2.62 ± 0.07	2.71 ± 0.05	2.98 ± 0.09
	$C_4 – I_2$	3	0.92 ± 0.02	0.98 ± 0.04	1.04 ± 0.03	1.21 ± 0.03
	$I_T – I_3$	4	0.63 ± 0.02	0.63 ± 0.03	0.62 ± 0.03	0.76 ± 0.03
	$C_3 – I_1$	5	0.92 ± 0.02	0.98 ± 0.01	1.04 ± 0.03	1.21 ± 0.02
	O – I_T	6	0.29 ± 0.01	0.34 ± 0.01	0.43 ± 0.01	0.45 ± 0.01

Equivalent gating charges calculated for model C14. Values are mean ± SEM (n = 6-9).

lel inactivated-states (I1–I2) consist of both entropic and enthalpic changes, suggesting that chemical bonds are reforming and conformational changes of the channel are taking place. For the C4–O transition there is a net decrease in enthalpy along with a net decrease in entropy when the channel goes from the last closed state C4 to the open state O (Table 7). This result suggests that the opening step corresponds to a reorganization of the channel with a decrease in the degrees of freedom of the molecule giving a more ordered system in the open state. While the energy barrier for O–I_T was increased by 5% in the mutant (Fig. 6, left), the one for C4–I2 was reduced down

Table 7. Parameters of the energy barriers.

		ΔH	ΔS	TΔS$_{20}$	ΔG10	ΔG25
C – C/I$_1$ – I$_2$	WT	56 ± 6	211 ± 18	62	-4 ± 8	-7 ± 8
	R1448H	43 ± 3	160 ± 11	47	-2 ± 4	-4 ± 5
C$_4$ – O/I$_2$ – I$_3$	WT	-52 ± 10	-131 ± 27	-38	-15 ± 13	-13 ± 13
	R1448H	-34 ± 15	-66 ± 39	-19	-16 ± 19	-15 ± 19
C$_3$ – I$_1$	WT	8 ± 7	87 ± 23	26	-17 ± 10	-19 ± 10
	R1448H	-8 ± 4	27 ± 12	8	-15 ± 5	-16 ± 5
C$_4$ – I$_2$	WT	42 ± 75	203 ± 131	60	-16 ± 84	-19 ± 85
	R1448H	-6 ± 10	31 ± 31	9	-15 ± 13	-16 ± 13
O – I$_T$	WT	88 ± 8	336 ± 25	99	-7 ± 11	-13 ± 11
	R1448H	74 ± 5	277 ± 9	81	-5 ± 6	-9 ± 6
I$_T$ – I$_3$	WT	-76 ± 9	-235 ± 24	-69	-10 ± 12	-6 ± 12
	R1448H	-81 ± 29	-251 ± 81	-73	-10 ± 37	-7 ± 38

ΔH (kJ /mol) and ΔS (J /Kmol) values were obtained by fitting Eq. 4 and Eq. 5 to α'i and β'i (i=1..6) values. TΔS20 (kJ /mol) was calculated for 20°C. ΔG10 and ΔG25 (kJ /mol) were calculated using ΔG = ΔH – TΔS for 10°C and 25°C respectively. Values are fit values ± SEM.

to 50%, 50 vs. 95 kJ/mol, confirming the facilitated transitions between C4 and I2 due to strikingly increased alpha3, i.e. meaning enhanced closed-state inactivation for R1448H (Fig. 6, right).

Single-channel behavior

Our finding that entry into rapid inactivation of R1448H was faster than for WT at threshold-near potentials (Fig. 3) was interpreted as tendency of R1448H channels to deactivate and inactivate through closed states. To further prove this hypothesis, the probability of transitions from O to I2 was modeled and it is obvious that this transition occurs in R1448H and not in WT (Fig. 7). Cooling shows a clear increase in the probability for this transition as expected from the whole-cell current data at lower temperatures.

The model's rate constants were used to calculate single-channel properties to determine whether the slowing of the current decay observed for R1448H can arise from longer open times or an increased number of openings. The estimated mean open times were up to 4-fold longer for R1448H than for WT. Cooling increased the mean open time of both R1448H and WT channels (Fig. 8 top). The bell-shaped curves showed open-time maxima between -50 and 0 mV. To the left of the maximum, the mean open time was dominated by the rate beta2 and to the right of the maximum by alpha6. This means that Na^+ channels open and close several times before they finally enter the inactivated state. Importantly the calculated number of openings was ~20% greater for R1448H than for WT (Fig. 8 bottom). Cooling reduced the number of re-openings for both WT and R1448H. In summary the slowed decay of whole-cell currents (Fig. 1) is due to an increase in open times which are further increased by cooling. The rate constants and the transition probabilities showed that the increased num-

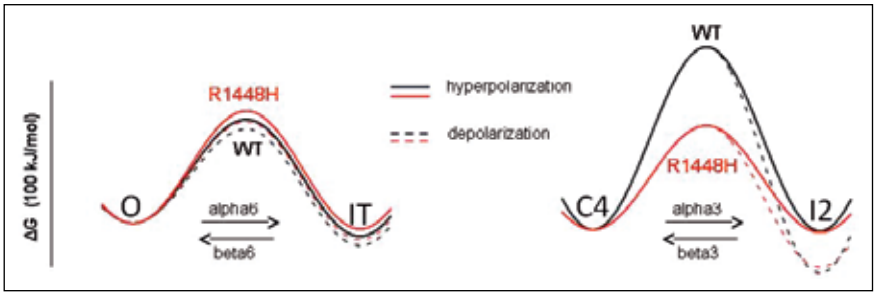

Figure 6. Free energy barriers between states. Total free energy barriers between states were calculated for -160 mV (solid line) and + 50 mV (scattered line) for WT (black) and R1448H (red). The value to the left of the energy barrier was set to 0 to allow direct comparison between curves. Note the very low barrier for the C4-I2 closed-sate inactivation transition (right) for the mutant. In contrast the O-IT open-state inactivation transition barrier is only very mildly elevated for the mutant (left).

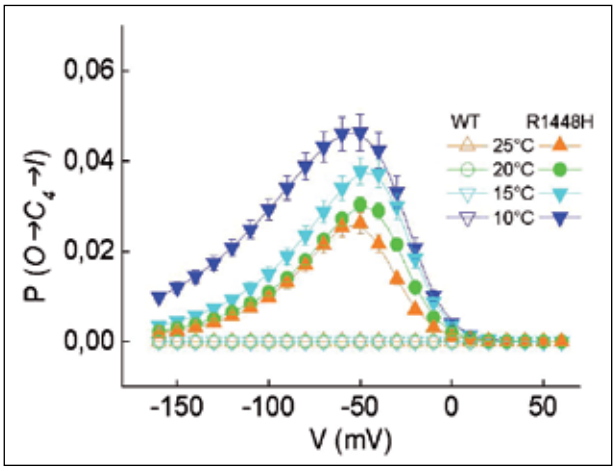

Figure 7. Voltage dependence of closed-sate inactivation probability. The probability for a transition from O → C4 → I2 was calculated according Eq. 8 for WT (open symbols) and R1448H (filled symbols) for 10°C-25°C. Values are mean ± SEM (n = 6-9). SEM is shown as bars when it exceeds the size of the symbol. Note that this transition practically does not occur in WT (P~0), but only in the mutant.

ber of R1448H openings is due to re-openings from the closed state C_4 and not from the inactivated states. As the mutant channel shows the minimum of the energy landscape for I3, the channels reach this state by the C4–I2 pathway instead of by IT. Mutant channels go along the O→C4→I2→I3 pathway.

Discussion

Our whole-cell data confirms previous studies in so far as R1448H slows open-state inactivation and shifts steady-state rapid inactivation to more negative potentials (3, 20-22) and that the seemingly temperature sensitivity in paramyotonia is a result of channel kinetics which are already slowed in the warmth and undergo a normal slowing with cooling (23, 24). Therefore, we assume that the required changes made to our model to best fit the data are not the result of our specific measurement or our set-up but rather reveal generally valid states and transitions.

The required introduction of the transient inactivated state IT into our model suggests that open-state inactivation may result from a two-step process. The two inactivation phases become more obvious at low temperatures whereas they cannot be temporally resolved at higher temperatures. A biphasic inactivation process is actually in agreement with the classical HH model and with previous single channel measurements (3). We interpret the two phases to be linked to deactivation and inactivation.

The required enabling of the C4 - I2 transition (which really occurs in the mutant only and not in WT) is mainly responsible for the channel re-openings of R1448H which are known to cause repetitive action potentials and paramyotonia. The transition rates and energy barriers of our model suggest that the re-openings originate from C4–O transitions and not from O–I transitions since the inactivation on-rate is reduced. This view is further evidenced by the enhanced inactivation from closed states, a slightly accelerated recovery from rapid inactivation, and the absence of a persistent current due to the limited number of re-openings by the increased rate of C_4-I_2 transi-

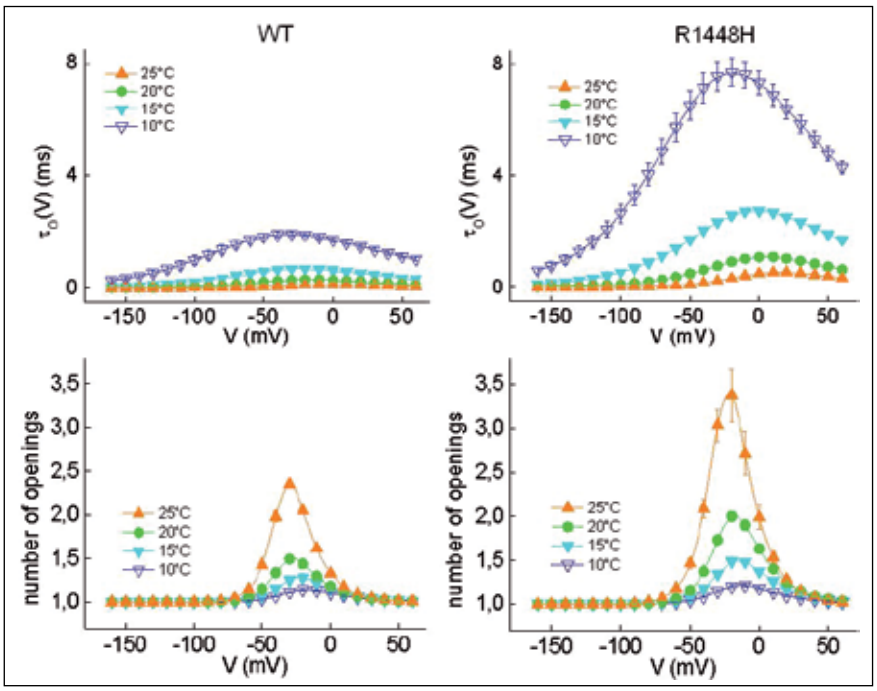

Figure 8. Temperature and voltage dependence of open times and number of openings. Temperature and voltage dependence of the mean open time (top) and the number of openings before inactivation (bottom) was calculated for indicated voltages for WT (left) and R1448H (right) between 10 and 25°C. Values are mean ± SEM (n = 6-9). SEM is shown as bars when it exceeds the size of the symbol. Note the elongated open time and the elevated number of openings in the mutant compared to WT.

tions. The enhanced deactivation has been previously also deduced (3).

As found previously for R1448H but not R1448C (3), closed-state inactivation (CSI) is strikingly enhanced for the R1448H mutation. We assume this is due to a more outward positioned resting-state S4 because of the eliminated positive charge at residue 1448 similar to calcium channel mutations (16). The enhanced CSI can explain the transition from myotonia to flaccid muscle weakness. Since R1448H impairs the movement of the voltage sensor, the receptor for the inactivation gate is more readily available for voltages around the activation threshold and less available for further depolarized voltages. The slowing of the rapid inactivation prolongs the duration of muscle action potentials as measured in vivo (25), whereby the combination of repetitive activity and prolonged duration of each action potential leads to a cold-induced depolarization and thus intracellular Na^+ accumulation that can even be detected by ^{23}Na magnetic resonance tomography in vivo (26, 27).

Acknowledgements

Frank Lehmann-Horn (FLH) and Karin Jurkat-Rott (KJR) receive grants from the non-profit Else Kröner-Fresenius-Stiftung, the German Federal Ministry of Education and Research (BMBF, IonoNeurOnet), and the German Muscle Disease Society (DGM). KJR is fellow of and FLH is endowed Senior Research Neuroscience Professor of the non-profit Hertie-Foundation.

References

1. Lehmann-Horn F, Jurkat-Rott K. Voltage-gated ion channels and hereditary disease. Physiol Rev 1999;79:1317-7.
2. Yang N, Ji S, Zhou M, et al. Sodium channel mutations in paramyotonia congenita exhibit similar biophysical phenotypes in vitro. Proc Natl Acad Sci USA 1994;91:12785-9.
3. Chahine M, Jr. George AL, Zhou M, et al. Sodium channel mutations in paramyotonia congenita uncouple inactivation from activation. Neuron 1994;12:281-94.
4. Armstrong CM. Na channel inactivation from open and closed states. Proc Natl Acad Sci 200&103:17991-6.
5. Horn R, Vandenberg CA. Statistical properties of single sodium channels. J Gen Physiol 1984;84:505-34.
6. Armstrong CM, Bezanilla F. Inactivation of the sodium channel. ii. gating current experiments. J Gen Physiol 1977;70:567-90.
7. Sheets MF, Hanck DA. Voltage-dependent open-state inactivation of cardiac sodium channels: gating current studies with anthopleurin-a toxin. J Gen Physiol 1995;106:617-40.
8. Yue DT, Lawrence JH, Marban E. Two molecular transitions influence cardiac sodium channel gating. Science 1989;244:349-52.
9. Irvine LA, Jafri MS, Winslow RL. Cardiac sodium channel Markov model with temperature dependence and recovery from inactivation. Biophys J 1999;76:1868-85.
10. Kahlig KM, Misra SN, Jr George AL. Impaired inactivation gate stabilization predicts increased persistent current for an epilepsy-associated scn1a mutation. J Neurosci 2006;26:10958-66.
11. Bean BP. Sodium channel inactivation in the crayfish giant axon. Must channels open before inactivating? Biophys J 1981;35:595-614.
12. Patlak J. Molecular kinetics of voltage-dependent Na+ channels. Physiol Rev 1991;71:1047-80.
13. Kuo CC, Bean BP. Na+ channels must deactivate to recover from inactivation. Neuron 1994;12:819-29.
14. Mitrovic N, Jr George AL, Lerche H, et al. Different effects on gating of three myotonia-causing mutations in the inactivation gate of the human muscle sodium channel. J Physiol 1995;487:107-14.
15. Alekov A, Rahman MM, Mitrovic N, et al. A sodium channel mutation causing epilepsy in man exhibits subtle defects in fast inactivation and activation in vitro. J Physiol 2000;529:533-9.
16. Kuzmenkin A, Hang C, Kuzmenkina E, et al. Gating of the hypopp-1 mutations: I. mutant-specific effects and cooperativity. Pflugers Arch 2007;454:495-505.
17. Stevens CF. Interactions between intrinsic membrane protein and electric field. an approach to studying nerve excitability. Biophys J 1978;22:295-306.
18. Colquhoun D, Hawkes AG. The principes of the stochastic interpretation of ion-channel mechanisms. In: Sakmann B, Neher E, editors. Single Channel Recordings. 2nd ed. New York: Plenum Publishing Corporation 1995.
19. Vandenberg CA, Bezanilla F. A sodium channel gating model based on single channel, macroscopic ionic, and gating currents in the squid giant axon. Biophys J 1991;60:1511-33.
20. Chen LQ, Santarelli V, Horn R, et al. A unique role for the s4 segment of domain 4 in the inactivation of sodium channels. J Gen Physiol 1996;108:549-56.
21. Dice MS, Abbruzzese JL, Wheeler JT, et al. Temperature-sensitive defects in paramyotonia congenital mutants r1448c and t1313m. Muscle Nerve 2004;30:277-88.
22. Mitrovic N, Jr George AL, Horn R. Role of domain 4 in sodium channel slow inactivation. J Gen Physiol 2000;115:707-18.
23. Lerche H, Mitrovic N, Dubowitz V, et al. Paramyotonia congenita: the r1448p Na+ channel mutation in adult human skeletal muscle. Ann Neurol 1996;39:599-608.
24. Featherstone DE, Fujimoto E, Ruben PC. A defect in skeletal muscle sodium channel deactivation exacerbates hyperexcitability in human paramyotonia congenita. J Physiol 1998;506:627-3.
25. Wagner S, Lerche H, Mitrovic N, et al. A novel sodium channel mutation causing a hyperkalemic paralytic and paramyotonic syndrome with variable clinical expressivity. Neurology 1997;49:1018-25.
26. Weber MA, Nielles-Vallespin S, Essig M, et al. Muscle Na+ channelopathies: Mri detects intracellular 23na accumulation during episodic weakness. Neurology 2006;67:1151-8.
27. Nagel AM, Amarteifio E, Lehmann-Horn F, et al. 3 Tesla sodium inversion recovery magnetic resonance imaging allows for improved visualization of intracellular sodium content changes in muscular channelopathies. Invest Radiol 2011;46:759-66.